Unfolding the physics of URu_2Si_2 through silicon to phosphorus substitution

A. Gallagher[1], K.-W. Chen[1], C.M. Moir[1], S.K. Cary[2], F. Kametani[3], N. Kikugawa[1,4], D. Graf[1], T.E. Albrecht-Schmitt[2], S.C. Riggs[1], A. Shekhter[1] & R.E. Baumbach[1]

The heavy fermion intermetallic compound URu_2Si_2 exhibits a hidden-order phase below the temperature of $17.5\,K$, which supports both anomalous metallic behavior and unconventional superconductivity. While these individual phenomena have been investigated in detail, it remains unclear how they are related to each other and to what extent uranium f-electron valence fluctuations influence each one. Here we use ligand site substituted $URu_2Si_{2-x}P_x$ to establish their evolution under electronic tuning. We find that while hidden order is monotonically suppressed and destroyed for $x \leq 0.035$, the superconducting strength evolves non-monotonically with a maximum near $x \approx 0.01$ and that superconductivity is destroyed near $x \approx 0.028$. This behavior reveals that hidden order depends strongly on tuning outside of the U f-electron shells. It also suggests that while hidden order provides an environment for superconductivity and anomalous metallic behavior, it's fluctuations may not be solely responsible for their progression.

[1] National High Magnetic Field Laboratory, Florida State University, Tallahassee, Florida 32310, USA. [2] Department of Chemistry and Biochemistry, Florida State University, Tallahassee, Florida 32306, USA. [3] Applied Superconductivity Center, Florida State University, Tallahassee, Florida 32310, USA. [4] National Institute for Materials Science 3-13 Sakura, Tsukuba 305-0003, Japan. Correspondence and requests for materials should be addressed to R.E.B. (email: baumbach@magnet.fsu.edu).

Materials that defy straightforward description in terms of either localized or itinerant electron behavior are a longstanding challenge to understanding novel electronic matter[1-4]. The intermetallic URu_2Si_2 is a classic example, where the itinerant electrons exhibit a giant magnetic anisotropy that is normally a characteristic of localized electrons[5,6]. URu_2Si_2 further displays an unknown broken symmetry state ('hidden-order') and unconventional superconductivity for temperatures below $T_0 = 17.5$ K and $T_c = 1.4$ K, respectively[7-10]. The development of new experimental techniques and access to ultra-high-purity single crystal specimens has recently advanced our understanding of the ordered states in this compound. For instance, excitations in the A_{2g} channel have been identified by electronic Raman spectroscopy as a signature of the hidden order[11], while elastoresistance[12], resonant ultrasound[13] (Ramshaw, B.J., Private communication.) and spectroscopic measurements[14] suggest the presence of fluctuations in the B_{2g}, B_{1g} and E_g channels, respectively. These studies follow high resolution X-ray diffraction[15], torque magnetometry[16] and polar Kerr effect measurements[17], which provide further insight into hidden order. It is also noteworthy that URu_2Si_2 differs from most other unconventional superconductors, which are typically found near the zero temperature termination point of a line of phase transitions, a 'quantum critical point,' where strong fluctuations are believed to be favourable for the superconducting pairing[18-21]. In contrast, the superconductivity in URu_2Si_2 is fully contained inside the ordered phase, as revealed by numerous tuning studies[22-33].

To explore the mechanisms of hidden order, anomalous metallic behavior and superconductivity in this material we synthesized high purity single crystal specimens of chemically substituted $URu_2Si_{2-x}P_x$, where ligand site substitution is a 'gentle' way to tune the electronic state. Recent advances developing a molten metal flux growth technique to produce high quality single crystal specimens of URu_2Si_2 enabled these experiments, which were previously inaccessible due to metallurgical challenges associated with the high-vapor pressure of phosphorus[34]. We report electrical transport and thermodynamic measurements, which reveal that while hidden order is destroyed for $x \leq 0.035$, the superconducting strength evolves non-monotonically with a maximum near $x \approx 0.01$ and that superconductivity disappears near $x \approx 0.028$. While the rapid suppression of hidden order indicates the importance of itinerant electrons, the unexpected maximum in superconducting strength may suggest the presence of a critical point that is defined by the termination of a phase boundary other than that of the hidden order. Owing to the relatively small chemical difference between silicon and phosphorus, we propose that in this series the dominant tuning effect is simply to change the chemical potential. Extrinsic factors such as disorder, as well as some intrinsic factors including changes in the unit cell volume or bond angles, spin orbit coupling and ligand hybridization strength play a minor role. Phosphorus substitution further has the advantage that it does not directly affect either the local electron count or the balance of the spin–orbit and Coulomb interactions of the d- or f-electrons on the Ru and U sites, making it an ideal and long desired tool for unraveling the physics of URu_2Si_2.

Results

Electrical transport and heat capacity. In Fig. 1 we show normalized electrical resistance R and heat capacity C versus temperature T for several phosphorus concentrations x (see Supplementary Fig. 1 for magnetic susceptibility $\chi(T)$). The Kondo lattice behavior of the electrical resistance (that is, non-monotonic temperature dependence below room temperature
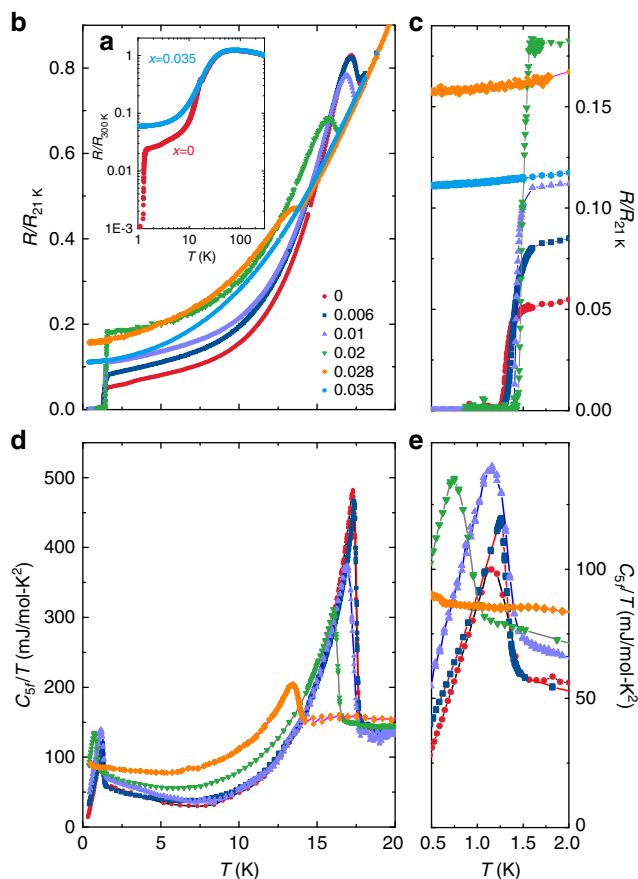

Figure 1 | Electrical transport and heat capacity for $URu_2Si_{2-x}P_x$.
(**a**) Electrical resistance normalized to the value at 300 K $R/R_{300\,K}$ versus temperature T for phosphorus concentrations $x = 0$ and 0.035. (**b**) Electrical resistance normalized to the value at 21 K $R/R_{21\,K}$ versus T for $0 \leq x \leq 0.035$. (**c**) $R/R_{21\,K}$ versus T in the low temperature region, emphasizing the superconducting transitions. (**d**) The $5f$ contribution to the heat capacity C_{5f} divided by T versus T for $0 \leq x \leq 0.028$. (**e**) C_{5f}/T versus T in the low T region, showing the bulk superconducting transitions. See Supplementary section for a description of the phonon background subtraction.

with a resistive peak near 80 K) for $T \geq T_0$ is unaffected by phosphorus substitution for $x \leq 0.035$ (Fig. 1a), suggesting that the strength of the hybridization between the f- and conduction electron states does not change much in the range $0 < x < 0.035$. At lower temperatures, the hidden order transition temperature T_0 and the size of the anomalies in R and C associated with it are monotonically suppressed with increasing x (Fig. 1b,d). There is an excellent agreement between the values of T_0 as extracted from R, C/T, and χ, indicating that disorder effects are negligible. We find no evidence for hidden order in $x = 0.035$ for $T > 20$ mK, showing that there is a quantum phase transition from hidden order to a paramagnetic correlated electron metal between $0.028 < x < 0.035$. However, the data does not preclude the possibility of a broad fluctuation regime around the quantum phase transition. The paramagnetic region subsequently extends up to $x \approx 0.25$ (nearly a factor of 10 larger x) where correlated electron antiferromagnetism appears (See Supplementary Fig. 2) (Results for the larger x $URu_2Si_{2-x}P_x$ substitution series will be reported separately). Unlike for other tuning strategies[22-33], magnetism is distant from hidden order in this phase diagram.

The resistive superconducting transition temperature $T_{c,\rho}$ (Fig. 1c) initially weakly increases with x and subsequently vanishes, with no evidence for bulk superconductivity above 20 mK for $x > 0.02$. While the value of $T_{c,C}$ extracted from heat

capacity is in close agreement with $T_{c,\rho}$ for $x \leq 0.01$, these values separate for $x = 0.02$, where $T_{c,\rho} > T_{c,C}$. We note that a similar discrepancy between $T_{c,\rho}$ and $T_{c,C}$ is seen for high quality single crystal specimens of the correlated electron superconductor CeIrIn$_5$ and may be an intrinsic feature of the unconventional superconducting state[35]. From both ρ and C/T, we find that for $x = 0.028$ there is a transition into the hidden order state near 13.5 K, but no bulk superconductivity down to 20 mK. There is no evidence for superconductivity in $x = 0.035$ for $T > 20$ mK.

Silicon to phosphorus phase diagram. These results are summarized in Fig. 2a, where the superconducting region is enclosed by hidden order in the $T - x$ phase space. Over this concentration range, the ground state is mainly tuned by electronic variation, as indicated by the comparably small changes in other intrinsic and extrinsic factors. The lowest residual resistivity ratio ($RRR \approx \rho_{300\,K}/\rho_0$) for the specimens reported here is $RRR = 10$ (see Supplementary Fig. 3), which is comparable with the typical values for parent URu$_2$Si$_2$, where T_0 and T_c depend weakly on RRR in the range 10–500 (ref. 34). The high crystal–chemical quality of these specimens is further highlighted by the observation of quantum oscillations in electrical transport measurements (see Supplementary Fig. 4), indicating that disorder effects are negligible. The unit cell volume and bond angles are also unchanged by phosphorus substitution (Fig. 2e), in contrast to some previous studies[26,27].

Having established the $T - x$ phase diagram (Fig. 2a), we now discuss the region beneath the hidden order phase boundary, where unexpectedly rich behavior occurs. As evidenced by the jump size in C_{5f}/T at T_c ($\Delta C_{5f}/T_c$) (and the transition width), which evolve though a maximum (and a minimum) between 0.006 and 0.01, respectively (Figs 1e and 2b), phosphorus substitution non-monotonically enhances the thermodynamic signature of the superconductivity. Here, C_{5f} refers to the heat capacity following subtraction of the nonmagnetic ThRu$_2$Si$_2$ lattice term, as described in the Supplementary section (Supplementary Fig. 5). The non-monotonic behavior is reflected in the behavior of $S_{5f,Tc}(x)$ (Fig. 2c), which goes through a maximum near $x = 0.01$. In contrast, for the hidden order $\Delta C/T_0$ and $S_{5f,T0}$ are monotonically suppressed with increasing x (see Supplementary Fig. 6). Further evidence for non-monotonic evolution of the superconductivity is provided by the doping evolution of the ratio $\zeta = \Delta C_{5f}/\gamma T_c(x)$, (Fig. 2b) which, for conventional superconductors, is a numeric constant $\zeta_{BCS} = 1.43$. By using C_{5f}/T at T_c for the value of the normal state γ we find that $\zeta(x)$ evolves non-monotonically through a maximum value of 1.2 at $x = 0.01$ (Fig. 2b), where the $x = 0$ value is near 0.7 as previously reported[18,19]. This suggests that the superconducting coupling strength may evolve through a maximum. We note that there is no evidence that all electrons from phosphorus substitution contribute directly to the conduction bands that are important for superconductivity.

Electrical transport in magnetic fields. Magnetoresistance data (Fig. 3) show quantum oscillations, emphasizing the high quality of these specimens (see Supplementary Fig. 4). Similar to the parent compound, the upper critical field H_{c2} (Fig. 3d) is highly anisotropic at all x and follows $H_{c2}(\theta) \propto 1/\sqrt{g_c^2 \cos^2\theta + g_a^2 \sin^2\theta}$ dependence (where θ is measured from the c-axis), suggesting that the upper critical field is Pauli limited[5]. While there is little x dependence in $g_c(x)$, the a-axis g-factor $g_a(x)$ significantly decreases before the superconductivity is destroyed near $x \approx 0.028$ (Fig. 3d). We note that the actual value of the g-factor in the a-direction may differ significantly from the fitted $g_a(x)$ because of the increased importance of diamagnetic effects as the field rotates into the ab-
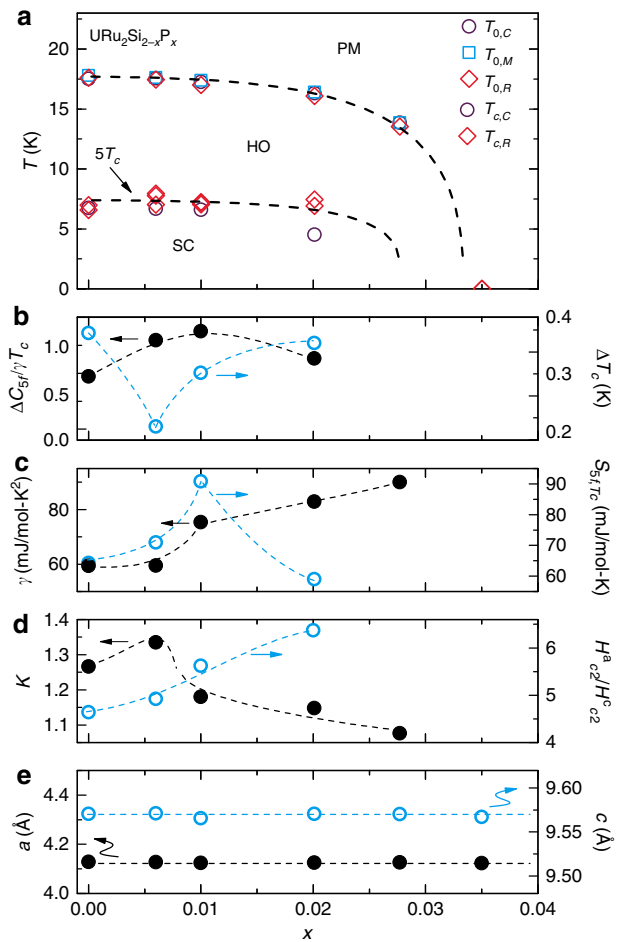

Figure 2 | Summary of physical quantities for URu$_2$Si$_{2-x}$P$_x$.
(**a**) Temperature T versus phosphorus concentration x phase diagram for URu$_2$Si$_{2-x}$P$_x$ constructed from heat capacity (circles), magnetic susceptibility (squares) and electrical resistance (diamonds). The $T - x$ phase boundary $T_0(x)$ separates the paramagnetic heavy electron liquid phase from the hidden order phase. $T_c(x)$ separates the hidden order and superconducting phases. The dotted lines are guides to the eye. (**b**) Left axis: The size of the discontinuity in the heat capacity divided by the superconducting transition temperature T_c and the electronic coefficient of the heat capacity γ, $\Delta C_{5f}/\gamma T_c$ versus x. Right axis: The width of the superconducting phase transition ΔT_c versus x. (**c**) Left axis: The electronic coefficient of the heat capacity γ versus x. Right axis: The $5f$ contribution to the entropy S_{5f} at T_c versus x. (**d**) Left axis: The value of the Kohler scaled curve at $H/R_0 = 50$ versus x. Right axis: The anisotropy of the upper critical field curves H_{c2}^a/H_{c2}^c versus x. (**e**) The lattice constants, $a(x)$ (left axis) and $c(x)$ (right axis), obtained from single crystal X-ray diffraction measurements.

plane. It remains to be seen whether these trends are consistent with recent theoretical proposals such as ref. 6.

Magnetoresistance measurements further highlight the non-monotonic evolution with x of the superconductivity and the underlying metallic state. Figure 3e demonstrates Kohler scaling for $H < 9$ T applied parallel to the c-axis at all dopings[36], suggesting that the magnetotransport is controlled by the same (temperature dependent) relaxation time as the zero field resistivity. At each composition in the range $0 < x < 0.028$ the normalized magnetoresistance is described by a distinct $f_x(h)$ (where $h = H/\rho(0, T)$), which itself evolves with doping. Notably, the function $f_x(h)$ evolves non-monotonically with x with a maximum near $x = 0.006$ (Fig. 2d). The maximum in the value of
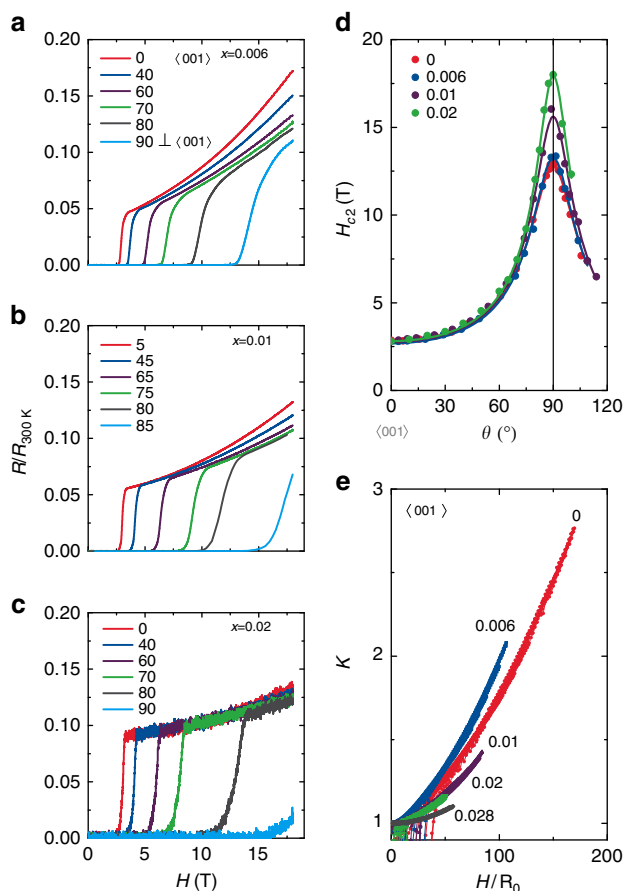
Figure 3 | Electrical transport in magnetic fields for URu$_2$Si$_{2-x}$P$_x$. (**a**) The $x = 0.006$ electrical resistance normalized to the room temperature value R/R_{300K} versus magnetic field H for several different angles θ. The data were collected at the temperature $T = 20$ mK. The electrical current was applied in the ab-plane and $\theta = 0$ is the configuration where, H is parallel (||) the crystallographic c-axis. (**b**) R/R_{300K} versus H for $x = 0.01$ at $T = 20$ mK for select θ. (**c**) R/R_{300K} versus H at $T = 20$ mK for $x = 0.02$ for select θ. (**d**) The upper critical field H_{c2}, defined as the extrapolated zero resistance intercept, for $T = 20$ mK for $0 \leq x \leq 0.02$. Data for $x = 0$ is from ref. 38. (**e**) The Kohler scaled electrical resistivity $K = \frac{\rho(H,T)}{\rho(0,T)}$ versus the reduced field H/R_0 for $0 \leq x \leq 0.028$.

$f_x(h)$ nearly coincides with the maximum in the thermodynamic signatures of the superconductivity inside the hidden order phase.

Discussion

Although much of the recent excitement surrounding URu$_2$Si$_2$ has focused on the uranium electronic structure and the symmetry of the hidden-order phase, a more fundamental question is the degree to which the f-electrons can be treated as being localized and the role of valence fluctuations. The continuity of experimental information extracted from well-developed applied pressure (P) and chemical substitution (x) series has proven essential to disentangle such effects in other correlated systems including high temperature superconducting cuprates, pnictides and heavy fermion compounds. To some extent, URu$_2$Si$_2$ has also benefited from such studies. For example, pressure drives a first order phase transition from hidden order into antiferromagnetism near $P_c = 0.5$ GPa, with a simultaneous evolution of the Fermi surface[22–25], but the resulting insight is limited by the small number of pressure-cell compatible experimental probes. Ruthenium site substitution

with Fe and Os produces $T - x$ phase diagrams that closely resemble the $T - P$ phase diagram[26–28], but the information gained from these series is constrained by strong disorder. Moreover, ruthenium site substitution is particularly disruptive, as evidenced by the rather different phase diagrams resulting from Rh and Re substitution studies where the hidden order and superconductivity are rapidly destroyed[29–33]. To understand the complex interplay between different phenomena in this compound a more 'gentle' tuning scheme has long been desired, which could provide access to the physics of URu$_2$Si$_2$ in clean single crystals at ambient pressure. In this context, ligand site substitution in URu$_2$Si$_2$ is an obvious target for investigation.

While in many theoretical scenarios for hidden order in URu$_2$Si$_2$ the U-5f electrons are treated as having mostly fixed valence in a particular atomic crystal field state[6,11], it is now believed that they have a dual character: that is, the dynamic nature of the U-5f valence electrons allows for fluctuations between different configurations. However, measurements of the pure compound so far give no insight into the role of these fluctuations in favouring hidden order and superconductivity. The rapid changes in the hidden order and superconductivity in our measurements confirm the importance of the itinerant electron states. This is further supported by the weak evolution of Kondo lattice physics[37] (which tracks the hybridization strength between f- and conduction electrons) and strong evolution in the g-factor anisotropy (which is a marker for local moment character). Together these results point towards this series as a platform for unraveling the relationship between local and itinerant behavior in URu$_2$Si$_2$.

The stark contrast in the evolution of the hidden order and superconductivity in URu$_2$Si$_{2-x}$P$_x$ (monotonic versus non-monotonic) further suggests that hidden order, although necessary, may not be directly responsible for the superconducting pairing. Instead, the observation of superconductivity completely contained inside the hidden order region and non-monotonic evolution of thermodynamic and electrical transport properties may indicate the presence of an independent collapsing phase boundary within the hidden order state, as is ubiquitous in other unconventional superconductors. This scenario is reinforced by the observed non-monotonic evolution of the normal state electrical transport, which is also common in correlated electron systems[18–21], where the strongest deviation from Fermi liquid behavior is seen near the critical point. Alternatively, the independent evolution of hidden order and superconductivity may suggest several competing order parameters in the hidden order phase, as evidenced by electronic Raman (A_{2g})[11], elastoresistance (B_{2g})[12], resonant ultrasound (B_{1g})[13](Ramshaw, B.J., Private communication.) and spectroscopic measurements (E_g)[14]. These studies should be extended into ligand site substituted URu$_2$Si$_2$.

Finally, the existing theoretical landscape focuses on f-electron physics with no guidance regarding the specificity of the transition metal ion. It is especially puzzling that hidden order and superconductivity are only observed in the U–Ru duo. Examination of silicon site substituted transition metal analogues (UT_2Si$_{2-x}$P$_x$, T = transition metal), which can now be synthesized using molten metal flux growth (We have already successfully synthesized several transition metal analogues UT_2Si$_2$ (T = Mn, Fe, Ir and Pt) using the same flux growth recipe.), may be particularly illuminating in addressing the universality of hidden order and superconductivity in this fascinating uranium compound.

Methods

crucible was then loaded into an alumina tube spanning the bore of a high-temperature horizontal tube furnace. Argon gas was passed through the tube and a zirconium getter was placed in a pot before the tantalum crucible in order to purify the argon at high temperatures. The crucible was heated to 500 °C at 50 °C/h, dwelled for 5 h, heated to 600 °C at 50 °C/h, dwelled for 5 h and heated to 1,450 °C at 70 °C/h. The dwells at intermediate temperature are intended to allow the phosphorus to completely dissolve into the indium flux without producing a dangerous high-vapor pressure. The crucible was then cycled between 1,450 and 1,400 °C at 100 °C/h 10 times. Finally, the furnace was turned off and quickly cooled to room temperature. The indium flux was subsequently removed using hydrochloric acid, to which the $URu_2Si_{2-x}P_x$ crystals are insensitive. This technique produced single-crystal platelets similar to the ones previously reported.

Bulk thermodynamic and electrical transport measurements. Heat capacity measurements were performed for mosaics of single crystals using the He3 option in a Quantum Design Physical Properties Measurement System for temperatures $400\,mK < T < 20\,K$. Magnetization $M(T, H)$ measurements were carried out for mosaics of single crystals for temperatures $T = 1.8$–$350\,K$ under an applied magnetic field of $H = 5\,kOe$ applied parallel to the c-axis using a Quantum Design Magnetic Property Measurement System. Magnetic susceptibility χ is defined as the ratio M/H. Zero magnetic field electrical resistance R was measured using the He3 option in Quantum Design Physical Properties Measurement System for temperatures $400\,mK < T < 300\,K$. Several individual crystals were measured for each concentration, which revealed a high degree of batch uniformity. The angular dependence of the superconducting upper critical field was measured using the superconducting magnet (SCM-1) dilution refrigerator system at the National High Magnetic Field Laboratory for $H < 18\,T$ and $T = 20\,mK$. Additional magnetoresistance measurements were performed at the National High Magnetic Field Laboratory, Tallahassee, up to magnetic fields of 35 T and at $T = 50\,mK$.

References

1. Herring, C. The state of d electrons in transition metals. *J. Appl. Phys.* **31,** S3 (1960).
2. Mott, N. in *Progress in Metal Physics* 3 (ed. Chalmers, B.) (London Pergamon Press, 1952).
3. Keimer, B., Kivelson, S. A., Norman, M. R., Uchida, S. & Zaanen, J. From quantum matter to high-temperature superconductivity in copper oxides. *Nature* **518,** 179 (2015).
4. Moore, K. T. & van der Laan, G. Nature of the 5f states in actinide metals. *Rev. Mod. Phys.* **81,** 235 (2009).
5. Altarawneh, M. M. *et al.* Superconducting pairs with extreme uniaxial anisotropy in URu2Si2. *Phys. Rev. Lett.* **108,** 066407 (2012).
6. Chandra, P., Coleman, P. & Flint, R. Hastatic order in the heavy-fermion compound URu2Si2. *Nature* **493,** 621 (2013).
7. Palstra, T. T. M. *et al.* Superconducting and magnetic transitions in the heavy-fermion system URu2Si2. *Phys. Rev. Lett.* **55,** 2727 (1985).
8. Schlabitz, W. *et al.* Superconductivity and magnetic order in a strongly interacting fermi-system: URu2Si2. *Z. Phys. B* **62,** 171 (1986).
9. Maple, M. B. *et al.* Partially gapped Fermi surface in the heavy-electron superconductor URu2Si2. *Phys. Rev. Lett.* **56,** 185 (1986).
10. Mydosh, J. A. & Oppeneer, P. M. Colloquium: Hidden order, superconductivity, and magnetism: The unsolved case of URu2Si2. *Rev. Mod. Phys.* **83,** 1301 (2011).
11. Kung, H.-H. *et al.* Chirality density wave of the "hidden order" phase in URu2Si2. *Science* **347,** 1339 (2015).
12. Riggs, S. C. *et al.* Evidence for a nematic component to the hidden-order parameter in URu2Si2 from differential elastoresistance measurements. *Nat. Commun.* **6,** 6425 (2015).
13. Yanagisawa, T. *et al.* Hybridization-driven orthorhombic lattice instability in URu2Si2. *Phys. Rev. B* **88,** 195150 (2013).
14. Wray, L. A. *et al.* Spectroscopic determination of the atomic f-electron symmetry underlying hidden order in URu2Si2. *Phys. Rev. Lett.* **114,** 236401 (2015).
15. Tonegawa, S. *et al.* Direct observation of lattice symmetry breaking at the hidden-order transition in URu2Si2. *Nat. Commun.* **5,** 4188 (2014).
16. Okazaki, R. *et al.* Rotational symmetry breaking in the hidden-order phase of URu2Si2. *Science* **331,** 439 (2011).
17. Schemm, E. R. *et al.* Evidence for broken time-reversal symmetry in the superconducting phase of URu2Si2. *Phys. Rev. B* **91,** 140506 (2015).
18. Löhneysen, H. v., Rosch, A., Vojta, M. & Wölfle, P. Fermi-liquid instabilities at magnetic quantum phase transitions. *Rev. Mod. Phys.* **79,** 1015 (2007).
19. Pfleiderer, C. Superconducting phases of f-electron compounds. *Rev. Mod. Phys.* **81,** 1551 (2009).
20. Tallon, J. L. & Loram, J. W. The doping dependence of T*—what is the real high-Tc phase diagram? *Physica C* **349,** 53 (2001).
21. Walmsley, P. *et al.* Quasiparticle mass enhancement close to the quantum critical point in BaFe2As$_{(1-x}$P$_x)_2$. *Phys. Rev. Lett.* **110,** 257002 (2013).
22. McElfresh, M. W. *et al.* Effect of pressure on competing electronic correlations in the heavy-electron system URu2Si2. *Phys. Rev. B* **35,** 43 (1987).
23. Amitsuka, H. *et al.* Effect of pressure on tiny antiferromagnetic moment in the heavy-electron compound URu2Si2. *Phys. Rev. Lett.* **83,** 5114 (1999).
24. Jeffries, J. R., Butch, N. P., Yukich, B. T. & Maple, M. B. Competing ordered phases in URu2Si2: Hydrostatic pressure and rhenium substitution. *J. Phys. Condens. Matt.* **20,** 095225 (2008).
25. Hassinger, E. *et al.* Similarity of the fermi surface in the hidden order state and in the antiferromagnetic state of URu2Si2. *Phys. Rev. Lett.* **105,** 216409 (2010).
26. Kanchanavatee, N. *et al.* Twofold enhancement of the hidden-order/large-moment antiferromagnetic phase boundary in the $URu_{2-x}Fe_xSi_2$ system. *Phys. Rev. B* **84,** 245122 (2011).
27. Kanchanavatee, N., White, B. D., Burnett, V. W. & Maple, M. B. Enhancement of the hidden order/large moment antiferromagnetic transition temperature in the $URu_{2-x}Os_xSi_2$ system. *Phil. Mag.* **94,** 3681 (2014).
28. Das, P. *et al.* Chemical pressure tuning of URu2Si2 via isoelectronic substitution of Ru with Fe. *Phys. Rev. B* **91,** 085122 (2015).
29. Amitsuka, H., Hyomi, K., Nishioka, T., Mitakato, Y. & Suzuki, T. Specific heat and susceptibility of $U(Ru_{1-x}Rh_x)_2Si_2$. *J. Mag. Magn. Mat.* **76,** 168 (1988).
30. Dalichaouch, Y. *et al.* Effect of transition-metal substitutions on competing electronic transitions in the heavy-electron compound URu2Si2. *Phys. Rev. B* **41,** 1829 (1990).
31. Dalichaouch, Y., Maple, M. B., Torikachvili, M. S. & Giorgi, A. L. Ferromagnetic instability in the heavy-electron compound URu2Si2 doped with Re or Tc. *Phys. Rev. B* **39,** 2423 (1989).
32. Bauer, E. D. *et al.* Non-Fermi-liquid behavior within the ferromagnetic phase in $URu_{2-x}Re_xSi_2$. *Phys. Rev. Lett.* **94,** 046401 (2005).
33. Butch, N. P. & Maple, M. B. The suppression of hidden order and the onset of ferromagnetism in URu2Si2 via Re substitution. *J. Phys. Condens. Matt.* **22,** 164204 (2010).
34. Baumbach, R. E. *et al.* High purity specimens of URu2Si2 produced by a molten metal flux technique. *Phil. Mag.* **94,** 3663 (2014).
35. Petrovic, C. *et al.* A new heavy-fermion superconductor CeIrIn5: A relative of the cuprates? *Europhys. Lett.* **53,** 354 (2001).
36. Kohler, V. M. Zur magnetischen Widerstandsänderung reiner Metalle. *Ann. Phys.* **32,** 211 (1938).
37. Hewson, A. C. *The Kondo Problem to Heavy Fermions* (Cambridge University Press, 1993).
38. Ohkuni, H. *et al.* Fermi surface properties and de Haas-van Alphen oscillations in both the normal and superconducting mixed states of URu2Si2. *Phil. Mag. B* **79,** 1045 (1999).

Author contributions

R.E.B., A.S. and S.C.R. conceived and designed the experiments and supervised measurements. A.G. synthesized single crystals. A.G., K.-W.C., C.M.M., N.K. and D.G. performed electrical transport and heat capacity measurements. F.K. performed chemical analysis measurements. S.K.C. and T.E.A.-S. performed single crystal x-ray diffraction measurements.

Additional information